Atmospheric and Climate Sciences, 2026, 16(3), 658-678
https://www.scirp.org/journal/acs
ISSN Online: 2160-0422
ISSN Print: 2160-0414

The Critical Role of Temperate Forests in the Modern Warming Period

Masaharu Nishioka

Independent Researcher, Chicago, IL, USA
Email: m.nishioka@sbcglobal.net

How to cite this paper: Nishioka, M. (2026) The Critical Role of Temperate Forests in the Modern Warming Period. *Atmospheric and Climate Sciences*, **16**, 658-678.
https://doi.org/10.4236/acs.2026.163033

Received: June 30, 2026
Accepted: July 27, 2026
Published: July 30, 2026

Abstract

The role of soil respiration (*Rs*) in the global carbon cycle has long been recognized. However, amidst the strong emphasis placed on the impact of anthropogenic carbon dioxide (CO_2) emissions on global warming, the role of *Rs* tends to be overlooked. The volume of CO_2 generated through *Rs* far exceeds that generated through anthropogenic emissions. Furthermore, *Rs* increases in tandem with increasing temperature (T). Consequently, in the current era of global warming, the CO_2 released through *Rs*, driven by rising temperatures, represents an additional quantity beyond the existing equilibrium level of atmospheric CO_2. Compared with tropical rainforests, *temperate forests* experience greater T fluctuations; as a result, the T dependence of *Rs* is more pronounced in these ecosystems. It is therefore believed that vegetation and temperate forests play decisive roles in influencing global warming. The specific role played by temperate forests, particularly in relation to T changes (ΔT) and the concomitant changes in CO_2 concentration (ΔCO_2), has been highlighted by our recent research findings. This role is now further corroborated by multiple results derived from satellite observations. We anticipate that future reports based on continued satellite measurements and analyses will provide further insights into this critical subject.

Keywords

Global Warming, Cross-Correlation, Time Lag, Temperate Forest, Modern Warm Period, Thermally Induced CO_2, Soil Respiration

1. Introduction

Earth's atmospheric temperature (T) fluctuates because of "natural factors", such as changes in solar activity and volcanic eruptions. However, simulations based on the latest climate models reveal that even when natural factors are considered, the temperature increase since the mid-19th century cannot be reproduced. Furthermore, only by adding the anthropogenic factor of greenhouse gas carbon dioxide (CO_2) emissions can results that are closer to actual observational data be obtained on the basis of the IPCC's (Intergovernmental Panel on Climate Change) Sixth Assessment Report [1].

The report used the extremely strong statement that "there is no doubt that human influence has caused global warming." This is because the history of climate change over the past several thousand years, physical mechanisms, and the results of advanced computer analysis suggest that "human activity is the cause". In short, the consensus is that "humans are emitting CO_2 at a rate that exceeds the natural CO_2 cycle, enveloping the Earth like a blanket and preventing heat from escaping".

Looking back over the Earth's long history, including ice ages spanning hundreds of thousands of years, the relationship between T and CO_2 may not be a simple one-way street where one comes first but rather may have a mutually amplifying *feedback* structure. When humans burn fossil fuels, atmospheric CO_2 concentrations first increase, and this increase in CO_2 produces a greenhouse effect, which in turn causes T to increase. In other words, the causal relationship may proceed in the following order: anthropogenic CO_2 emissions → increase in CO_2 concentrations → increase in T. In this case, in modern global warming, the increase in CO_2 concentrations precedes the increase in T.

The cross correlation between T and CO_2 is among the fundamental starting points for addressing the issue of climate change. The commonly assumed relationship, as asserted by the IPCC, is that increases in CO_2 cause increases in T. However, analyses since 1990 have shown that the generally assumed relationship is in the opposite direction [2]-[10], casting doubt on this assumption. All the evidence from these analyses suggests a unidirectional relationship, with T as the cause and CO_2 as the effect. This relationship is not represented in climate models, which show an inverse correlation that is contradicted by actual measurements. These analyses revealed that CO_2 fluctuations lagged behind correlated changes in T by *several months* [2]-[10].

Therefore, in a series of recent studies, the correlation, causality, and causes of the correlation between T and CO_2 have been investigated [11]-[18]. The cause and core of the correlation is that, in contrast to the commonly held belief that "T increases are primarily caused by increases in CO_2 due to human activity," we have confirmed, using the latest observational data and statistical time series analysis, that "changes in T precede changes in CO_2 concentration" with a time lag. The results of these series of studies are reviewed in some detail below. To subsequently verify the results obtained and the mechanisms of global warming, we will examine several findings currently being gathered through satellite observations.

2. Discussion

Summary of previous studies

The correlation coefficient r between two variables, x and y, is defined by Equation (1) below. r ranges from −1 to 1, where the closer r is to 1, the stronger the correlation. As a guideline, a correlation coefficient of 0.8 or higher indicates a strong correlation, a correlation coefficient of 0.7 - 0.5 indicates a fair correlation, and a correlation coefficient of 0.4 - 0.3 indicates little correlation. The correlation coefficient r can be calculated relatively easily using the built-in function in Microsoft Excel®.

$$r = \frac{\frac{1}{n}\sum_{i=1}^{n}(x_i - \bar{x})(y_i - \bar{y})}{\sqrt{\frac{1}{n}\sum_{i=1}^{n}(x_i - \bar{x})^2}\sqrt{\frac{1}{n}\sum_{i=1}^{n}(y_i - \bar{y})^2}} \quad (1)$$

Murry Salby analyzed the temperature change (ΔT) and the rate of change in CO_2 concentration (ΔCO_2) and proposed that the relationship between ΔCO_2 and ΔT can be expressed as Equation (2) [19] [20]:

$$\mathrm{d}(\Delta CO_2)/\mathrm{d}t = \gamma \Delta T \ (\gamma\text{: a constant}) \quad (2)$$

The ΔCO_2 (annual change) values are reported by NOAA as visualized on their website [21], which they call the CO_2 growth rate. The ΔT (monthly average anomalies) and the growth rate during 1979/7 and 2023/12 are shown in **Figure 1(a)** [18]. The correlation coefficient r is 0.744. Although the high r can be interpreted as indicating a very good correlation, it should be noted that the same annual change value ΔCO_2 is used throughout each year. The power spectral density obtained via Fourier transforms for ΔT and ΔCO_2 is shown in **Figure 1(b)** [18]. A regular frequency pattern is observed in both. Furthermore, upon comparison of the double-headed arrows on the two power spectra in **Figure 1(b)**, a phase shift is observed between these frequencies.

A good correlation between ΔT and ΔCO_2 is shown in **Figure 1(a)**, but effective analysis is not possible when the time lag between these variables is less than 12 months. Therefore, we compared the 13-month monthly average ΔT with the 13-month monthly average ΔCO_2. It is necessary to download NOAA data and calculate the 13-month monthly average of ΔCO_2. As shown in **Figure 2(a)**, the correlation coefficient r between the two is 0.664 [17], indicating that ΔCO_2 changes with lag time (months). The value at which the correlation coefficient r is maximized indicates that ΔCO_2 changes with lag time. Therefore, Equation (2) can be rewritten as Equation (3).

$$\mathrm{d}(\Delta CO_2)/\mathrm{d}t = \gamma \Delta T' \ \ (\Delta T' = \Delta T \text{ when a lag time is considered}) \quad (3)$$

The power spectrum represents the intensity of the vibrational components of a signal at each frequency. However, it does not contain information about the phase (time difference), so it cannot determine the direction of the time difference. To quantitatively analyze the time difference, a cross-correlation function or cross-spectrum (cross-spectral density) must be used. Dedicated software is required to automate calculations using the cross-correlation function or cross-spectrum.

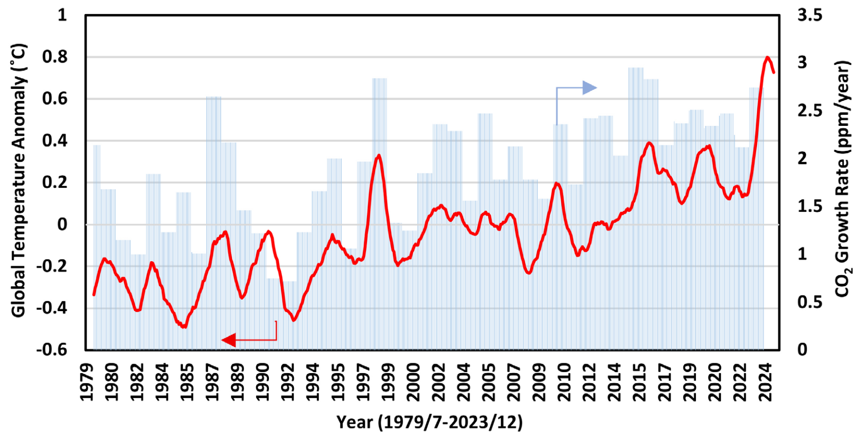

(a)

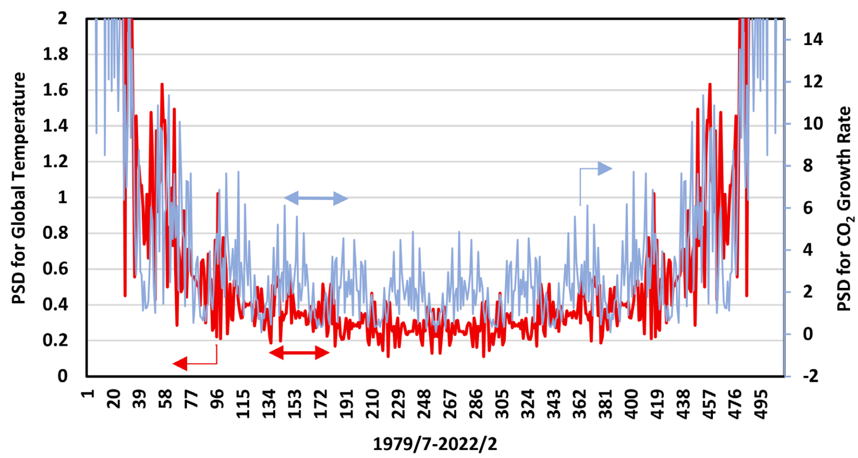

(b)

Figure 1. (a) Correlations of the global temperature anomaly (red line, scale: left axis, ˚C) and 12-month average annual CO_2 growth rates (blue bar, scale: right axis, ppm/year); (b) comparison of the power spectral density (PSD) obtained via Fourier transform for the global temperature anomaly and 12-month average annual CO_2 growth rates (the horizontal axis represents the number of data points from the start of the analysis. The number of data points is the same as the number of months [18].

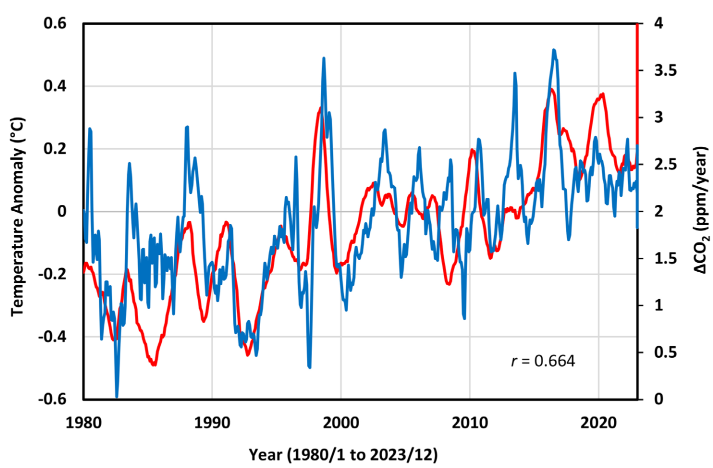

(a)

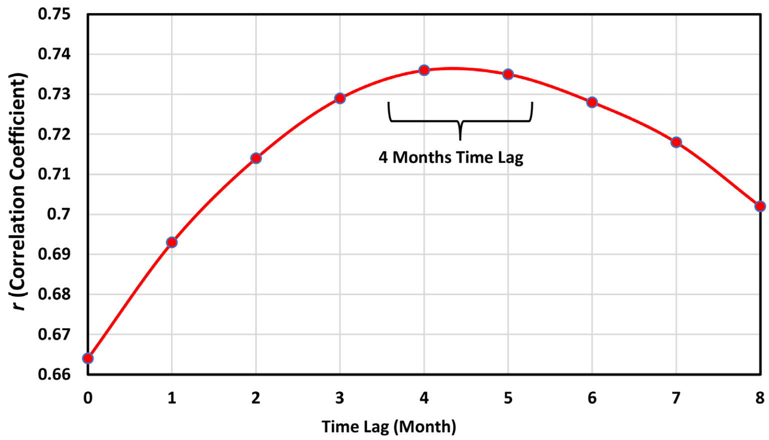

(b)

Figure 2. (a) Correlations between global temperature anomalies (red line, scale: left axis, ˚C) and *monthly* CO_2 annual growth rates (ΔCO_2, blue line, scale: right axis, ppm/year) and (b) changes in correlation coefficients with time lag (in months) [17].

Satellite measurements of Earth's temperature began in 1979, providing reliable information on ΔT over a large surface area. Moreover, long-term measurements of CO_2 concentrations have been ongoing since 1957 at an observatory on Mauna Loa, Hawaii, providing reliable ΔCO_2 data. As shown in **Figure 2(a)**, these reliable data clearly show that ΔT and ΔCO_2 have been well correlated since at least 1979, but ΔT leads ΔCO_2. The relationship between r and time lags is shown in **Figure 2(b)**. ΔT leads ΔCO_2 by approximately four months when the value of the maximized *r is considered*. Whether ΔT leads ΔCO_2 on longer timescales remains a challenge for further observation. If a change in the time lag does occur, it should be possible to detect it using the power spectrum.

When time series data are analyzed using a Fourier transform, if the time lag reverses midway, the "phase difference (phase spectrum)" calculated from the power spectrum will also reverse accordingly. However, because a normal Fourier transform processes the "entire period" all at once, some ingenuity is required to capture phenomena where the properties change midway. The details are beyond the scope of this paper, but one example is a method of dividing the data into short windows and performing a Fourier transform while shifting those windows. This makes it possible to track changes such as "the phase is positive in this time period and negative in the next time period."

ΔT and ΔCO_2 have been well correlated since at least 1979, but ΔT leads ΔCO_2 by approximately four months. The fact that ΔT precedes ΔCO_2 was also confirmed using a slightly different method [14]. ΔT and ΔCO_2 were analyzed before and after ENSO events. Owing to seasonal changes in photosynthesis and soil respiration (Rs), CO_2 concentrations follow a regular pattern, reaching their lowest values in August and their highest values in May each year. Therefore, as shown in **Figure 3**, we considered the CO_2 concentration and T changes over one year from September as a cycle for each year. T increases with the occurrence of El Niño. CO_2 concentrations also increase with increasing temperature. The values of ΔCO_2

and ΔT were calculated by comparing the El Niño period with the period before occurrence and were analyzed according to Equation (2). The correlation coefficient r was maximized by shifting ΔT by five months (Figure 4(a) and Figure 4(b)). ΔT and ΔCO_2 in Figure 4(b) overlap well *when* ΔT *is shifted* by five months. This indicates that ΔCO_2 is determined by ΔT, and the time lag is five months.

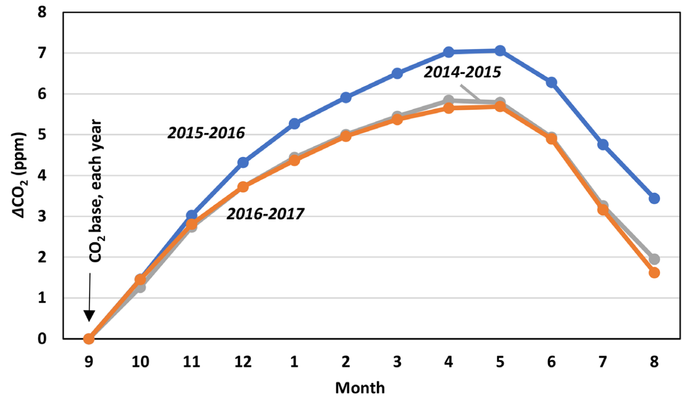

Figure 3. Changes in the annual CO_2 concentrations (ppm) from September 2014, 2015, or 2016 to August 2015, 2016, or 2017 [14].

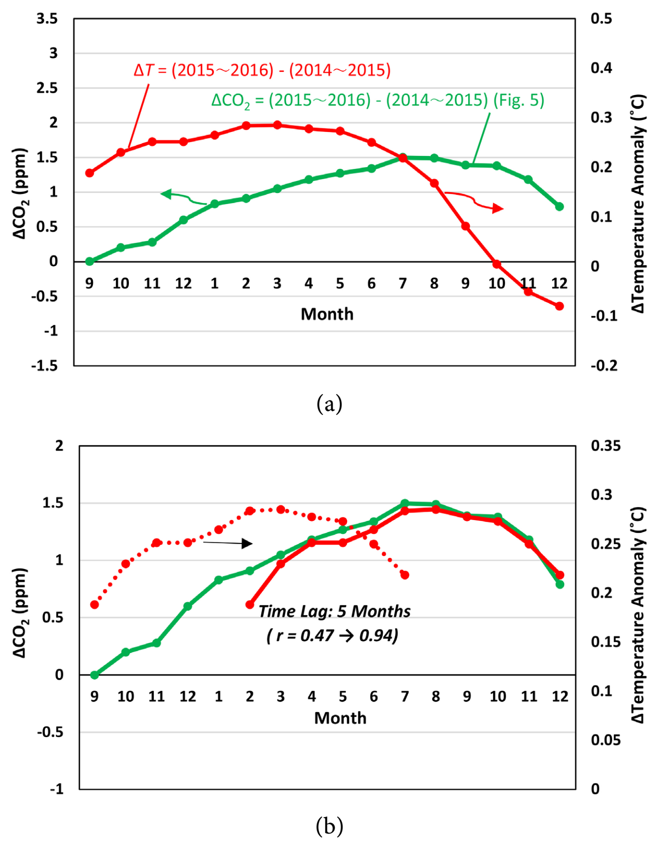

Figure 4. (a) Deviations in ΔCO_2 and ΔT between 2015-2016 and 2014-2015; (b) the same data are plotted, but ΔT is shifted to the right by five months. The correlation coefficient r is improved from 0.47 to 0.94 by shifting [14].

As demonstrated by the findings outlined above, since satellite-based observations of T began in 1979, changes in ΔCO_2 have consistently lagged behind changes in ΔT by a period of four to five months. Specifically, when T rose, CO_2 increased; conversely, when T fell, CO_2 decreased. During the major El Niño event of 1997-1999, as illustrated in **Figure 5**, ΔT shifted by 0.5˚C, whereas ΔCO_2 shifted by 2 ppm. Although the Earth released CO_2 when T rose, it subsequently absorbed that CO_2 back into the system as T cooled and returned to its baseline level.

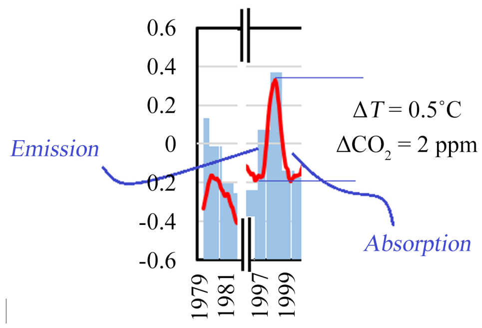

Figure 5. Changes in global temperatures and CO_2 concentration growth rates during El Niño events from 1997-99.

ΔCO_2 has consistently lagged behind ΔT by a period of four to five months since 1979. Therefore, whether anthropogenic ΔCO_2 affects ΔT is questionable. This question is also supported on the basis of a mass balance in the carbon cycle. The carbon cycle budget reported by the IPCC [1] is shown in **Figure 6**. Some critical numbers regarding anthropogenic CO_2 are summarized here [12].

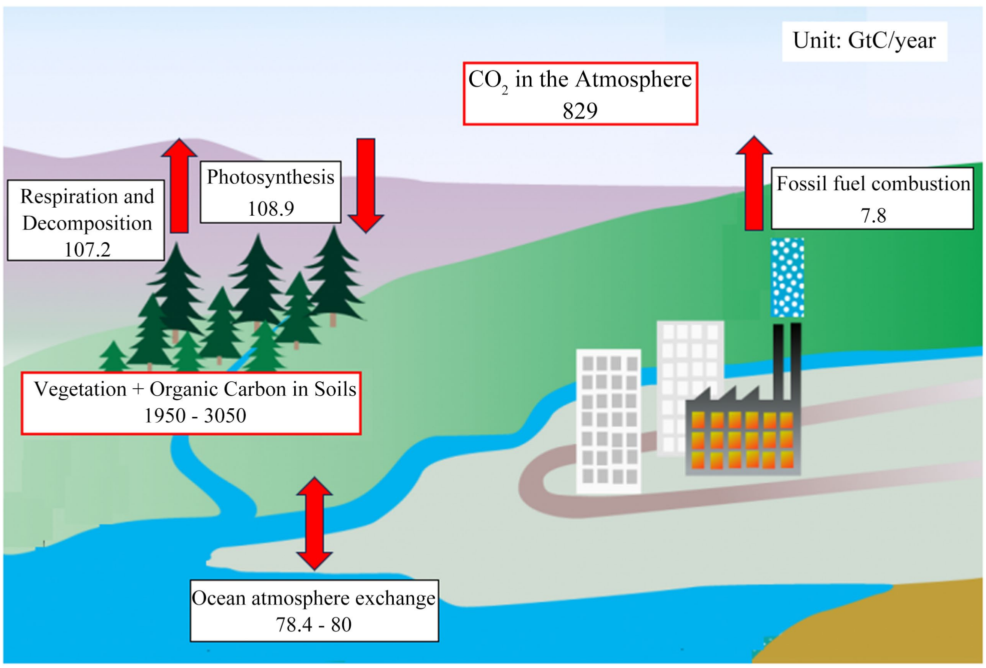

Figure 6. Simplified carbon cycles and carbon equivalent estimates (Unit: GtC) obtained from the IPCC report [12].

1) The carbon cycle budget shows that anthropogenic CO_2 accounts for only 4% of the total:

anthropogenic CO_2 ratio
≒ (fossil fuel combustion)/(fossil fuel combustion + respiration and decomposition + ocean atmosphere exchange)
≒ (7.8)/(7.8 + 107.2 + 79.2)
≒ 0.04 (4)

2) The residence time of CO_2 is approximately 4 years:

CO_2 residence time
= (CO_2 in the atmosphere)/(fossil fuel combustion + respiration and decomposition + ocean-atmosphere exchange)
≒(829)/(7.8 + 107.2 + 79.2)
≒4 (5)

3) CO_2 is only 4% of greenhouse gas, and the remaining 96% is H_2O:

CO_2 concentration in the greenhouse gas
≒(0.04)/(1 + 0.04)
≒0.04 (6)

Next, the results from our papers are summarized to investigate why ΔCO_2 has lagged behind ΔT by a period of four to five months since 1979. First, ΔCO_2 and ΔT at various latitudes were analyzed [11].

There are two major differences between the Northern and Southern Hemispheres [22]. The first, as illustrated in **Table 1**, lies in the disparity between their respective oceanic and land areas. Approximately 68% of the Earth's total landmass is concentrated in the Northern Hemisphere, where the proportion of land is more than double that of the Southern Hemisphere. In the Southern Hemisphere, however, more than 80% of the surface area is covered by ocean. In particular, the region between 40˚ and 60˚ south latitude is renowned as a zone where powerful westerly winds sweep across the sea unimpeded by landmasses.

Table 1. Proportions of ocean and land areas in the northern and southern hemispheres [22].

Region	Land area	Ocean area
Northern hemisphere	≈39%	≈61%
Southern hemisphere	≈19%	≈81%
Entire earth	≈29%	≈71%

Because land heats up and cools down more rapidly than water does, the Northern Hemisphere, which contains a greater proportion of landmass, tends to experience larger annual temperature fluctuations than the Southern Hemisphere. The Southern Hemisphere is characterized by the ease with which large-scale ocean currents develop, such as the Antarctic Circumpolar Current, precisely because it is not obstructed by massive continents.

The second point concerns the disparity in forest area between the Northern and Southern Hemispheres. Next, on the basis of data such as the latest Global Forest Resources Assessment (FRA 2020) by the Food and Agriculture Organization (FAO) of the United Nations [23], we compiled the forest area ratios. The total global forestland area is approximately 4 billion hectares (approximately 31% of the total land area). When categorized into "tropical rainforests" and "other forests," breakdown generally yields the following ratios (**Table 2**).

Table 2. Proportion of "Tropical Rainforests" and "Other Forests" [23].

Forest category	Proportion (Approx.)	Key characteristics
Tropical rainforests	**≈45%**	Amazon, Congo Basin, Southeast Asia, etc.
Other forests	**≈55%**	Subarctic (Taiga), Temperate, and Subtropical forests

Note: Among the "other forests" category, "subarctic forests" (boreal forests), which occupy a particularly vast area across the Northern Hemisphere, alone account for approximately 27% of the total.

The Northern Hemisphere is characterized by its extensive landmass, which encompasses the vast coniferous forest belts of Siberia and Canada; consequently, the proportion of "other forests" is overwhelmingly high. Tropical rainforests account for approximately 25% of the total, covering regions such as Central America, parts of North Africa, and portions of Southeast Asia. The remaining 75% consists of "other forests," comprising vast temperate forests as well as boreal forests, the largest forest zone on Earth. In contrast, while the landmass of the Southern Hemisphere is limited, the vast majority of its existing forests are located within the tropics. Tropical rainforests constitute approximately 70% of this total, with massive rainforest ecosystems, such as those covering the majority of the Amazon Basin, the Congo Basin, and Indonesia, concentrated in these regions. "Other forests" make up the remaining 30%, consisting of temperate and arid-zone forests found in countries such as Australia, Chile, Argentina, and South Africa. This creates a contrasting structural dynamic: the Northern Hemisphere serves as a "treasure trove of vast boreal and temperate forests," whereas the Southern Hemisphere acts as a "stronghold of tropical rainforests". In particular, the "other forests" of the Northern Hemisphere, specifically its boreal forests, play a role that is comparable to that of tropical rainforests, not only as carbon dioxide sinks but also in terms of the immense quantities of carbon stored within their soils.

On the basis of the aforementioned differences between the Northern and Southern Hemispheres, we can examine the variations in ΔCO_2 and ΔT at various latitudes, as presented in **Table 3**. Among these observations, points #4 and #5 in **Table 3** are crucial for addressing the following question: "Why does ΔCO_2 lag behind ΔT by four to five months?" Specifically, the magnitude of ΔCO_2 at approximately 50˚ north latitude is greater than that at the equator.

Table 3. Summary of the results obtained in study [11].

Number	Results
1	Temperature change correlates with the change rate of CO_2 concentration across latitudes from north to south.
2	Temperature change in the tropics strongly responds to El Niño.
3	A trend of the temperature increase is greater in the north (20 N - 90 N) than in the south (20 S - 90 S).
4	The change rate of CO_2 concentration at sine latitudes 0.75 (≒50 N) responds to temperature change more than in the tropics.
5	The change rate of CO_2 concentration at sine latitudes 0.75 (≒50 N) significantly responds to temperature change regardless of ENSO occurrences.
6	The difference of temperature change between land and ocean is larger in the south (20 S - 90 S) than in the north (20 N - 90 N).

Furthermore, the following results have been obtained [12].

1) δ^{13}C and ΔCO_2 are inversely correlated, which is known as the Suess effect [24]. However, natural CO_2, rather than anthropogenic CO_2, may affect the Suess effect more because anthropogenic CO_2 accounts for only 4%, as shown above.

2) The extent of the correlation between $d(\Delta CO_2)/dt$ and ΔT differs depending on the latitude and between the land and sea.

3) During El Niño, $d(\Delta CO_2)/dt$ follows ΔT with a time lag of several months, and CO_2 emission and absorption at the Earth's surface respond to ΔT.

4) The concentrations of CO_2, CH_4, and N_2O gases increase annually, but seasonal changes are observed. These concentrations decrease from spring to summer but increase from fall to winter.

5) *Rs* is interpreted to be activated in spring because of increasing temperatures and to generate CO_2, CH_4, and N_2O in fall because of biological processes after a time lag.

6) The temperature patterns have changed over the last 2000 years, as reflected by the ice age and warm periods. Therefore, CO_2 has evolved to breathe slowly in response to ΔT.

7) Plant decomposition and *Rs* are accompanied by microbial processes and increased soil fertility, and Earth is becoming greener because of rising CO_2 and increasing fertility.

On the basis of these results, we conclude that changes in plant decomposition and *Rs* due to global temperatures primarily control global CO_2 cycles. The impact of CO_2 emissions from fossil fuel combustion on global warming is extremely low. For these reasons, the man-made global warming hypothesis needs to be carefully reinvestigated.

As summarized above, $d(\Delta CO_2)/dt$ follows ΔT with a time lag of several months, and CO_2 emission and absorption at the Earth's surface respond to ΔT. The increase in ΔCO_2 with increasing ΔT can be regarded as *thermally induced* CO_2, which may be significantly related to *Rs*.

We investigated the impact of selected global conditions on *Rs*, drawing upon the latest NASA databases [13]. The variation in the annual carbon flux derived from *Rs* (g·C·m^{-2}) in relation to the annual mean temperature (˚C) over the period from 1961 to 2017 is shown in **Figure 7**. *Rs* has an approximately linear relationship with temperature. As noted above, ΔT influences *Rs*, thereby triggering changes in CO_2 production. The results presented in **Figure 7** demonstrate a positive correlation between *Rs* and temperature, thereby substantiating the aforementioned hypothesis.

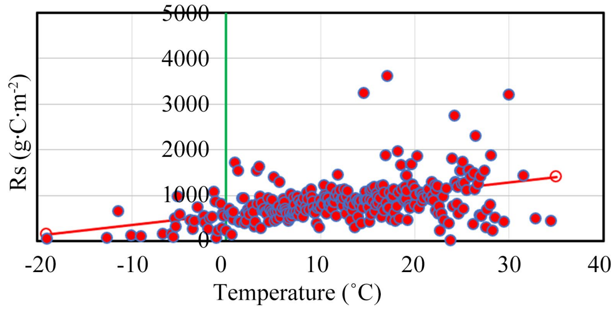

Figure 7. Change in annual *C* flux (g·C·m^{-2}) from soil respiration (*Rs*) versus mean annual temperature (˚C) between 1961 and 2017 (coefficient of determination (r^2): 0.172). The regression red line is $y = 23.3x + 582.0$ [13].

While CO_2 concentrations have been increasing annually, seasonal variations have been observed in previous studies [13]. Specifically, CO_2 concentrations decrease from spring to summer but increase from autumn to winter. *Rs* is interpreted as becoming active in the spring in response to rising temperatures and subsequently generating CO_2 through biological processes in the autumn following a certain time lag [13]. The seasonal variations in *Rs* flux (mean value: μmol·m^{-2}·s^{-1}) for spring, summer, autumn, and winter at the observation sites within the United States are listed in **Table 4**. The values on the vertical (*y*) axis in **Figure 8** represent ΔRs (=*Rs* flux − mean *Rs* flux) at each observation site. These results corroborate the interpretation of previous studies, namely, *Rs* becomes active in the spring, reaches a maximum value in the summer, and declines in the winter. Furthermore, these findings suggest that a time lag occurs in the fluctuations in CO_2 concentrations.

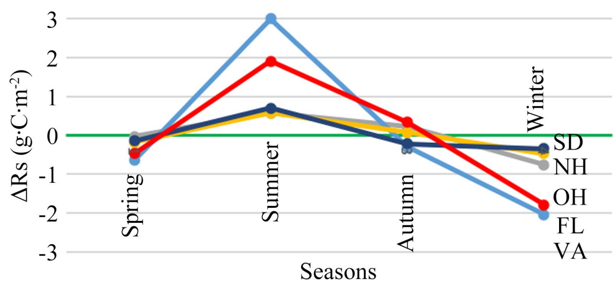

Figure 8. Mean seasonal *Rs* flux (μmol·m^{-2}·s^{-1}) in spring, summer, autumn, or winter in the U.S. The vertical values are the ΔRs (*Rs* flux − averaged *Rs* flux) at each site [13].

Table 4. Mean seasonal *Rs* flux ($\mu mol \cdot m^{-2} \cdot s^{-1}$) in spring, summer, autumn, or winter at US sites. ($\Delta Rs = Rs$ flux − averaged *Rs* flux) [12].

State	Location	Year		Spring	Summer	Autumn	Winter
OH	Morgan County	2005	*Rs*	1.09	1.69	1.34	0.36
			Δ*Rs*	−0.03	0.57	0.22	−0.76
VA	Blady Experimental Farm	2004	*Rs*	2.31	5.94	2.64	0.91
			Δ*Rs*	−0.64	2.99	−0.31	−2.04
NH	White Mountain National Forest	1998	*Rs*	0.49	1.25	0.74	0.21
			Δ*Rs*	−0.19	0.58	0.07	−0.46
SD	Northern Great Plains	2011	*Rs*	0.33	1.17	0.25	0.12
			Δ*Rs*	−0.14	0.70	0.22	−0.34
FL	Tall Timbers Research Station	2010	*Rs*	2.56	4.93	3.36	1.24
			Δ*Rs*	−0.46	1.91	0.34	−1.78

In *the Rs control process*, the increase in temperature due to the modern warm period increases CO_2 emissions *because of the increase in Rs*, *as* presented in Figure 9 [13]. One of the main factors is that the *Rs* control process in the *midlatitude forest zone* changes significantly because of temperature changes, such as those in temperate forests in Olympic National Park, WA (USA) (Figure 10). The emitted CO_2 can be considered thermally induced CO_2. As a result, the CO_2 concentration in the atmosphere increases. Therefore, although there is a cross-correlation between temperature and CO_2 concentration, *a temperature-leading time lag* is observed because it is a process mediated by *Rs*. Even though anthropogenic CO_2 has decreased, reducing total atmospheric CO_2 concentrations during the modern warm period is difficult. Additionally, this means that an increase in anthropogenic CO_2 since the Industrial Revolution has contributed too little to affecting the global CO_2 concentration.

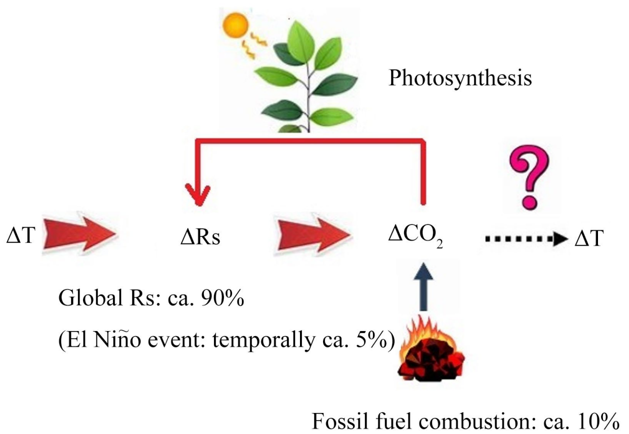

Figure 9. The *Rs* control process causes ΔCO_2 because of ΔT followed by changes in *Rs* [13].

Figure 10. Temperate forests in Olympic National Park, WA (USA) (photographed by the author, March 4, 2025).

The temperature tends to increase more in the north (20 N - 90 N) than in the south (20 S - 90 S), as shown above (see Table 3). Additionally, compared with that in the tropics, the rate of change in the CO_2 concentration at a sine latitude of 0.75 (≒50 N) corresponds to the degree of temperature change. For these reasons, temperate forests play a critical role in controlling *Rs*.

Satellite data with respect to Rs and CO_2 emissions in high-latitude regions

The impact of T fluctuations on CO_2 emissions is more pronounced in temperate forests than in tropical rainforests, where T variability is lower. Because temperate forests experience lower T than tropical rainforests, their rate of *Rs* is slower, resulting in carbon being sequestered within the soil over extended periods. However, as global warming causes T to increase, the decomposition rate of carbon-containing components sequestered in the soil accelerates. The impact of ΔT is more significant in temperate forests than in tropical rainforests, which exhibit less T variability. Therefore, the effects of global warming on the CO_2 balance differ between temperate forests and tropical rainforests, as determined by the following equation.

$$CO_2 \text{ Balance} = \text{Photosynthesis Rate} - (Rs + \text{Others}) \tag{7}$$

As T increases, the rate of *Rs* increases. Generally, the magnitude of the T dependence of *Rs* is characterized by the following equation [25]:

$$Q_{10} = \left(\frac{R_2}{R_1}\right)^{10^\circ\text{C}/(T_2 - T_1)} \tag{8}$$

(R_1 and R_2 are the respiration rates at temperatures T_1 and T_2 (˚C), respectively.)

A Q_{10} of 2 means that the *Rs* rate doubles for every 10˚C increase. In many ecosystems, the Q_{10} for *Rs* is ~1.5 - 2.0 (see Table 5) [26]**.** Other studies have also shown a tendency for Q_{10} values to increase with increasing latitude [27]. On the basis of data from chamber observations, a method involving placing a container over the ground to measure emissions spanning thousands of sites, the report establishes the statistical fact that Q_{10} values are higher at higher latitudes.

Table 5. Comparison of Rs and Q_{10} in temperate and tropical rainforests [26].

Forest type	Average soil respiration (gC/m^2/yr)	Typical Q_{10} range	Characteristics
Temperate forest	400 - 800	2.0 - 3.0	Fluctuates more significantly in response to temperature changes at lower temperature ranges.
Tropical rainforest	1000 - 1500	1.2 - 2.0	Response to temperature changes is relatively dampened.

With respect to Rs and CO_2 emissions, phenomena observable through satellite data, observational techniques and analytical methods have been steadily accumulating in recent years. Analyses utilizing gross/net primary production (GPP/NPP) data from NASA's MODIS instruments (the Terra and Aqua satellites) have revealed a phenomenon at mid-to-high latitudes: while increasing T in early spring stimulates photosynthesis, increasing T in early autumn and during nighttime hours drives an increase in Rs at an even faster rate [28].

Data from OCO-2 and OCO-3 (Orbiting Carbon Observatory satellites), which directly measure atmospheric CO_2 concentrations, reveal whether a specific region acts as a "CO_2 sink" or a "CO_2 source". Analyses have revealed a phenomenon occurring in temperate forest regions during recent periods of high T, in which CO_2 emissions resulting from Rs exceed CO_2 uptake through photosynthesis, leading to localized increases in CO_2 concentrations [29].

The NOAA Arctic Report Card (2024 edition) presents data indicating that in the permafrost regions of Alaska and Siberia, CO_2 emissions from the soil during the autumn and winter are beginning to exceed CO_2 uptake by vegetation during the summer [30].

The Global Carbon Project (GCP) compiles data on variations in the terrestrial carbon balance by latitude [31]. It provides statistical data concerning the impact that accelerated decomposition of soil organic matter in high-latitude regions has on the global carbon balance.

According to data analysis from OCO-2 and GOSAT ("Ibuki"), the increase in CO_2 concentrations during winter is greater in the high latitudes of the Northern Hemisphere than at the equator [32] [33]. *The* ΔCO_2 values at 50 N and in the tropics between 2019 and 2022 are compared in **Figure 11**, and the approximate values are shown in **Table 6**. While precise comparisons of ΔCO_2 are difficult, it is evident that compared with those at the equator, CO_2 levels at 50 N show a more pronounced increase in 2019. Although this difference may amount to only approximately 2.5 ppm, as shown above, it represents a significant disparity when viewed against the global average annual increase in CO_2 of 2 ppm.

Table 6. Comparison of *the* ΔCO_2 values at 50 N and in the tropics between 2019 and 2022.

At 50 N	April 2019 → April 2022
CO_2 (ppm)	412.5 - 417.5 → 420 - 425
ΔCO_2 (ppm)	2.5 - 12.5
At Tropical	**April 2019 → April 2022**
CO_2 (ppm)	412.5 - 415.0 → 417.5 - 422.5
ΔCO_2 (ppm)	0 - 10

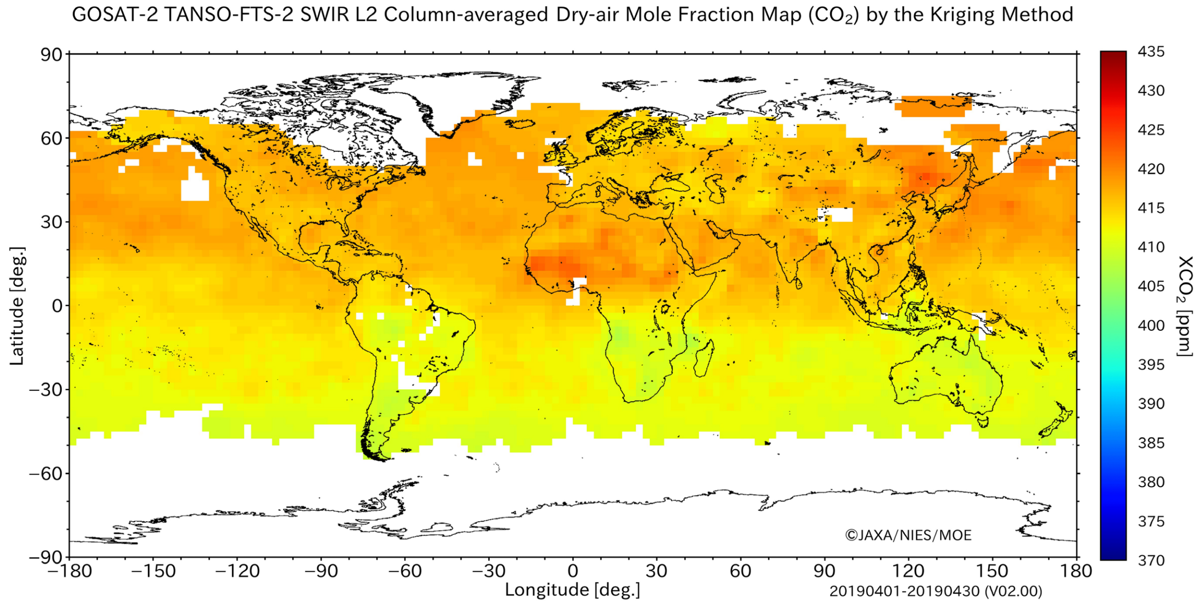

(a)

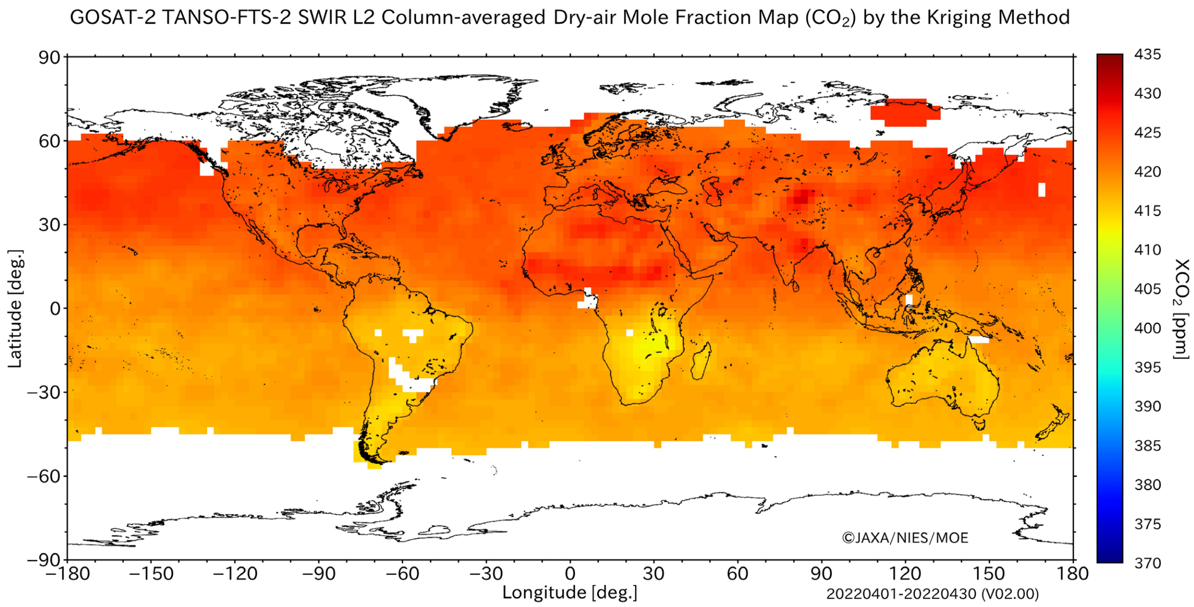

(b)

Figure 11. Global mapping of greenhouse gases retrieved from GOSAT Level 2 products, (a) duration: 4/1/2019-4/30/2019 and (b) duration: 4/1/2022-4/30/2022 [32].

Since 2015, land CO_2 uptake north of 20 N has decreased by half to 1.13 ± 0.24 GtC·yr^{-1} by 2023. Moreover, the tropics recovered from the 2015-2016 El Niño carbon loss, gained carbon during the La Niña years (2020-2023), and then switched to carbon loss during the 2023 El Niño (0.56 ± 0.23 GtC·yr^{-1}) [34].

Confirmation of Global Greening by Satellite Data

Owing to global warming, CO_2 emissions from soil in high-latitude regions are increasing, as summarized in the previous section. Satellite data also revealed that the world is greener than it was in the early 1980s. The updated maps in **Figure 12** show that the trend has continued [35]. This map shows where greenness increased (green) and decreased (brown) across the planet between 2000 and 2018. Specifically, the trends in the *leaf area index* (LAI) and the amount of leaf area relative to the ground area during the growing season are shown. There is a clear greening trend in boreal and Arctic regions, which is a result of increasing T. For example, Svalbard in the high Arctic has experienced a 30% increase in greenness. The greening was concurrent with an increase in the mean summer temperature from 2.9˚C to 4.7˚C between 1986 and 2015 [35].

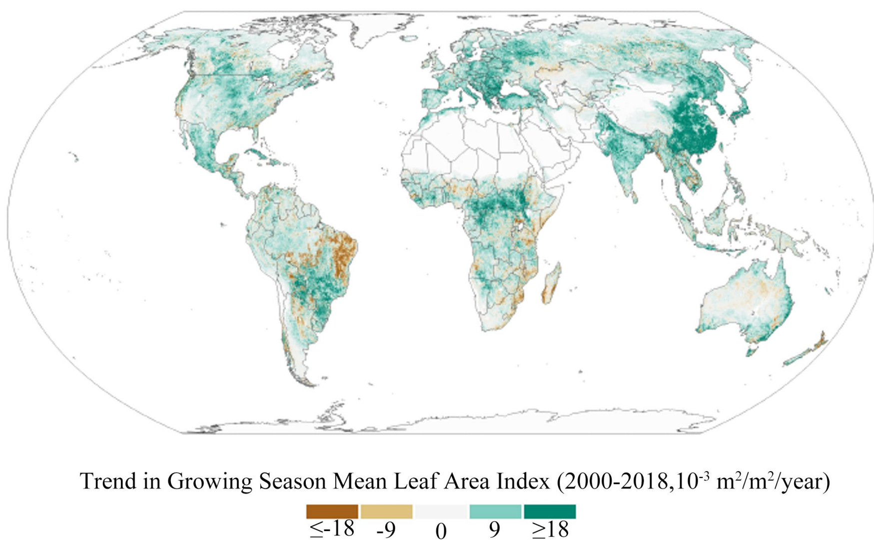

Figure 12. Trends in the glowing season mean leaf area index (2000-2018, 10^{-3}/m^2/year) [35].

Research teams, including those at NASA, have published analytical results corroborating greening by using satellite data [36] [37]. Over the approximately 35 to 40 years spanning from the early 1980s to the present day, it has been confirmed that the LAI of the Earth's vegetation has increased by 25% to 50%. The increase in LAI resulting from this greening is estimated to be approximately twice the land area of the entire United States, or approximately 1.5 times the size of the Amazon rainforest. A map of the world highlighting these newly greened areas is featured in NASA's explanatory materials [36]. Furthermore, this greening is attributed to the "CO_2 fertilization effect", which is the process by which increasing concentrations of CO_2 stimulate plant photosynthesis [37].

With the Google Earth Engine (time series comparison), decades' worth of satellite imagery overlaid as a time lapse can be viewed. If you visit "Google Earth Engine Timelapse" and zoom in on northern Alaska or the vicinity of the Siberian taiga boundary, you can observe how areas that were once dominated by snow and bare rock gradually become covered in green vegetation, specifically shrubs and grasses, year after year.

In the "Terrestrial Snow Cover" and "Tundra Greenness" sections of the NOAA Arctic Report Card, data are presented to demonstrate the correlation between rising temperatures and vegetation change characteristics at high latitudes, as shown in **Figure 13** [38].

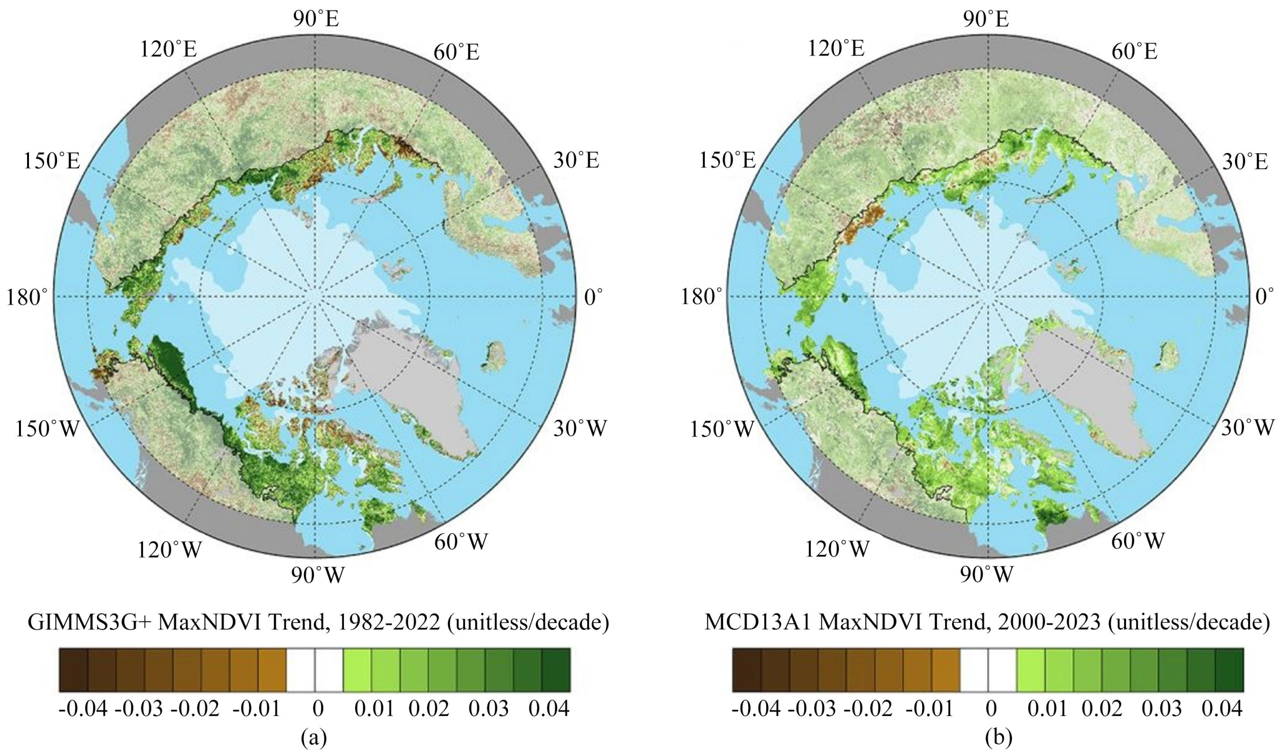

Figure 13. Magnitude of the maximum NDVI trend calculated as the change per decade using ordinary least squares regression for Arctic tundra (solid colors) and boreal forest north of 60˚ latitude (muted colors) during (a) 1982-2023 based on the AVHRR GIMMS 3-g+ dataset and (b) 2000-24 based on the MODIS MCD13A1 v6.1 dataset. In each panel, the circumpolar tree line is indicated by a black line, and the 2024 mean August sea-ice extent is indicated by light shading [36].

The normalized difference vegetation index (NDVI) is the most widely used indicator of "greenness," utilizing the absorption of red light and the reflection of near-infrared light by plant leaves. The LAI is an indicator of the total leaf area per unit of ground area, thereby reflecting changes in vegetation density. This method is under development [39]. Analysis utilizing Japanese satellite data, such as that from "Shikisai" (GCOM-C), is also currently advancing [40].

3. Concluding Remarks

Summarized in bullet points, the conclusions are as follows:

1) ΔT precedes ΔCO_2.

2) Global warming increases Rs, leading to increased CO_2 emissions from the soil.

3) The higher the latitude is, the greater the temperature dependence of CO_2 emissions from the soil.

4) The temperature dependence of CO_2 emissions in *temperate forests* is greater than that in *tropical rainforests*.

5) At high latitudes, *greening* is more temperature dependent because of global warming and the fertilization effect of CO_2.

6) The role of soil respiration in the global carbon cycle has long been recognized. However, amidst the emphasis placed on the impact of anthropogenic CO_2 emissions on global warming, the role of soil respiration tends to be overlooked. The amount of CO_2 generated by soil respiration far exceeds that generated by anthropogenic emissions; furthermore, compared with tropical rainforests, temperate forests exhibit greater temperature dependence in terms of soil respiration because of the magnitude of their temperature fluctuations. Consequently, vegetation, particularly temperate forests, is believed to play a decisive role in influencing global warming.

The role of temperate forests in relation to ΔT and the subsequent ΔCO_2 was highlighted by our recent research findings. Furthermore, this role has now been corroborated by several results derived from satellite observations. Further reports based on satellite measurements and analyses are anticipated in the future.

Conflicts of Interest

The author declares no conflicts of interest regarding the publication of this paper.

References

[1] https://www.ipcc.ch/assessment-report/ar6/

[2] Kuo, C., Lindberg, C. and Thomson, D.J. (1990) Coherence Established between Atmospheric Carbon Dioxide and Global Temperature. *Nature*, **343**, 709-714. https://doi.org/10.1038/343709a0

[3] Martín, F., Valero, F. and García-Miguel, J.A. (1994) On the Response of the Background Atmospheric CO_2 Growth Rate to the Anomalies of the Sea-Surface Temperature in the Equatorial Pacific Ocean. *Atmospheric Environment*, **28**, 517-530. https://doi.org/10.1016/1352-2310(94)90128-7

[4] Dettinger, M.D. and Ghil, M. (1998) Seasonal and Interannual Variations of Atmospheric CO_2 and Climate. *Tellus B*, **50**, 1-24. https://doi.org/10.1034/j.1600-0889.1998.00001.x

[5] Adams, J.M. and Piovesan, G. (2005) Long Series Relationships between Global Interannual CO_2 Increment and Climate: Evidence for Stability and Change in Role of the Tropical and Boreal-Temperate Zones. *Chemosphere*, **59**, 1595-1612. https://doi.org/10.1016/j.chemosphere.2005.03.064

[6] Park, J. (2009) A Re-Evaluation of the Coherence between Global-Average Atmospheric CO_2 and Temperatures at Interannual Time Scales. *Geophysical Research Letters*, **36**, L22704. https://doi.org/10.1029/2009gl040975

[7] Humlum, O., Stordahl, K. and Solheim, J. (2013) The Phase Relation between Atmospheric Carbon Dioxide and Global Temperature. *Global and Planetary Change*, **100**, 51-69. https://doi.org/10.1016/j.gloplacha.2012.08.008

[8] Wang, W., Ciais, P., Nemani, R.R., Canadell, J.G., Piao, S., Sitch, S., *et al.* (2013) Variations in Atmospheric CO_2 Growth Rates Coupled with Tropical Temperature. *Proceedings of the National Academy of Sciences of the United States of America*, **110**, 13061-13066. https://doi.org/10.1073/pnas.1219683110

[9] Koutsoyiannis, D., Onof, C., Kundzewicz, Z.W. and Christofides, A. (2023) On Hens, Eggs, Temperatures and CO_2: Causal Links in Earth's Atmosphere. *Sci*, **5**, Article 35. https://doi.org/10.3390/sci5030035

[10] Koutsoyiannis, D. (2024) The Relationship between Atmospheric Temperature and Carbon Dioxide Concentration. *Science of Climate Change*, **4**, 39-49.

[11] Nishioka, M. (2024) Changes in Temperature and CO_2 in the Atmosphere at Various Latitudes. *Current Research in Environmental Science and Ecology Letters*, **1**, 1-9.

[12] Nishioka, M. (2024) Effects of Plant Decomposition and Soil Respiration on CO_2 in the Atmosphere via Global Temperature Changes. *Current Research in Environmental Science and Ecology Letters*, **1**, 1-12.

[13] Nishioka, M. (2024) Effects of Anthropogenic Co_2 and Thermally-Induced CO_2 on Global Warming. *Atmospheric and Climate Sciences*, **14**, 317-327. https://doi.org/10.4236/acs.2024.143020

[14] Nishioka, M. (2024) Cross-Correlation between Global Temperature and Atmospheric CO_2 with a Temperature-Leading Time Lag. *Atmospheric and Climate Sciences*, **14**, 484-494. https://doi.org/10.4236/acs.2024.144029

[15] Nishioka, M. (2025) Relationship between the Standardized Precipitation Index and Global Temperature on the North American Continent. *Atmospheric and Climate Sciences*, **15**, 321-329. https://doi.org/10.4236/acs.2025.152016

[16] Nishioka, M. (2025) Difficulties in Reducing Atmospheric CO_2 Concentrations during the Modern Warm Period. *Atmospheric and Climate Sciences*, **15**, 451-461. https://doi.org/10.4236/acs.2025.152023

[17] Nishioka, M. (2025) Time Lag in Changes in Global Temperature and CO_2 Concentration Following Changes in the Oceanic Niño Index. *Atmospheric and Climate Sciences*, **15**, 668-680. https://doi.org/10.4236/acs.2025.153033

[18] Nishioka, M. (2026) Time Lag and Amplitude Differences between Correlated Variables in Global Temperature Changes. *Atmospheric and Climate Sciences*, **16**, 71-82. https://doi.org/10.4236/acs.2026.161005

[19] Salby, M. (2016) Atmospheric Carbon. Video Presentation, University College London. https://www.youtube.com/watch?v=3q-M_uYkpT0

[20] Salby, M. (2018) What Is Truly behind the Increase of Atmospheric CO2? Video Presentation, Helmut-Schmidt-University Hamburg. https://www.youtube.com/watch?v=rohF6K2avtY

[21] NOAA: Trends in Atmospheric Carbon Dioxide (CO_2). https://gml.noaa.gov/ccgg/trends/gr.html

[22] Wikipedia: Hemispheres of Earth. https://en.wikipedia.org/wiki/Hemispheres_of_Earth

[23] The Food and Agriculture Organization of the United Nations: Global Forest Resources Assessment 2020—Main Report. https://www.sprep.org/sites/default/files/documents/publications/forest-resources-

assessment-main-report.pdf

[24] Wikipedia: Suess Effect. https://en.wikipedia.org/wiki/Suess_effect

[25] Wikipedia: Q_{10} (Temperature Coefficient). https://en.wikipedia.org/wiki/Q10_(temperature_coefficient)

[26] Jian, J., Vargas, R., Anderson-Teixeira, K., Stell, E., Herrmann, V., Horn, M., *et al.* (2021) A Restructured and Updated Global Soil Respiration Database (SRDB-V5). *Earth System Science Data*, **13**, 255-267. https://doi.org/10.5194/essd-13-255-2021

[27] Raich, J.W. and Schlesinger, W.H. (2001) Global Annual Soil Respiration Data (Raich and Schlesinger 1992) (Version 1). ORNL Distributed Active Archive Center. https://doi.org/10.3334/ORNLDAAC/622

[28] Piao, S., Ciais, P., Friedlingstein, P., Peylin, P., Reichstein, M., Luyssaert, S., *et al.* (2008) Net Carbon Dioxide Losses of Northern Ecosystems in Response to Autumn Warming. *Nature*, **451**, 49-52. https://doi.org/10.1038/nature06444

[29] Das, S., Kiel, M., Laughner, J., Osterman, G., O'Dell, C.W., Taylor, T.E., *et al.* (2025) Comparisons of the V11.1 Orbiting Carbon Observatory-2 (OCO-2) X_{CO2} Measurements with GGG2020 TCCON. *Earth and Space Science*, **12**, e2024EA003935. https://doi.org/10.1029/2024ea003935

[30] NOAA in the Arctic. https://arctic.noaa.gov/report-card/

[31] Global Carbon Project. http://www.globalcarbonatlas.org/

[32] National Institute for Environmental Studies: GOSAT-2 Project. https://www.gosat-2.nies.go.jp/

[33] Watanabe, H., Hayashi, K., Saeki, T., Maksyutov, S., Nasuno, I., Shimono, Y., *et al.* (2015) Global Mapping of Greenhouse Gases Retrieved from GOSAT Level 2 Products by Using a Kriging Method. *International Journal of Remote Sensing*, **36**, 1509-1528. https://doi.org/10.1080/01431161.2015.1011792

[34] Ke, P., Ciais, P., Sitch, S., Li, W., Bastos, A., Liu, Z., *et al.* (2024) Low Latency Carbon Budget Analysis Reveals a Large Decline of the Land Carbon Sink in 2023. *National Science Review*, **11**, nwae367. https://doi.org/10.1093/nsr/nwae367

[35] NASA Earth Observatory (2020) Global Green up Slows Warming. https://science.nasa.gov/earth/earth-observatory/global-green-up-slows-warming-146296/

[36] Hille, K.B. (2016) Carbon Dioxide Fertilization Greening Earth, Study Finds. NASA https://www.nasa.gov/centers-and-facilities/goddard/carbon-dioxide-fertilization-greening-earth-study-finds/

[37] Zhu, Z., Piao, S., Myneni, R.B., Huang, M., Zeng, Z., Canadell, J.G., *et al.* (2016) Greening of the Earth and Its Drivers. *Nature Climate Change*, **6**, 791-795. https://doi.org/10.1038/nclimate3004

[38] NOAA: Arctic Report Card: Update for 2024. https://arctic.noaa.gov/report-card/report-card-2024/tundra-greenness-2024/

[39] NASA EARTHDATA. https://www.earthdata.nasa.gov/topics/land-surface/normalized-difference-vegetation-index-ndvi

[40] JAXA: Global Change Observation Mission—Climate "SHIKISAI" (GCOM-C). https://global.jaxa.jp/projects/sat/gcom_c/

Abbreviations

ENSO: El Niño-Southern Oscillation

IPCC: Intergovernmental Panel on Climate Change (the United Nations body)

NOAA: National Oceanic and Atmospheric Administration

NASA: National Aeronautics and Space Administration

LAI: Leaf Area Index

Rs: Soil Respiration

r: correlation coefficient